Mott insulator-superfluid phase transition in a detuned multi-connected Jaynes-Cummings lattice

SEO Kangjun & TIAN Lin*

School of Natural Sciences, University of California, Merced, California 95343, USA;

The connectivity and tunability of superconducting quantum devices provide a rich platform to build quantum simulators and study novel many-body physics. Here we study quantum phase transition in a detuned multi-connected Jaynes-Cummings lattice, which can be constructed with superconducting circuits. This model is composed of alternatively connected qubits and cavity modes. Using a numerical method, we show that by varying the detuning between the qubits and the cavities, a phase transition from the superfluid phase to the Mott insulator phase occurs at commensurate fillings in a one-dimensional array. We study the phase transition in lattices with symmetric and asymmetric couplings, respectively.

1 Introduction

Quantum simulation has become a frontier in quantum information science after it was first studied in the pioneer work of Feynman [1]. State-of-the-art technologies in building atomic and solid-state devices in the quantum limit enable us to build quantum simulators with rich controllability and novel physics effects [2]. Among such efforts, superconducting quantum simulation is being intensively explored in recent theoretical and experimental works. With superconducting circuits that contain only one or two qubits, people have demonstrated Anderson localization, switch of the Chern number in a topological phase transition, and the simultaneous coupling of a superconducting resonator to multiple qubits [3–6]. These experiments are enabled by technological developments in controlling and coupling superconducting devices with long decoherence times and high gate fidelity in the past decade [7–12]. Meanwhile, the experimental progress is paralleled by theoretical proposals on building both digital and analog quantum simulators with superconducting circuits. The many-body models be-

ing studied include quantum spin systems [13–18], models bearing novel topological properties [19–22], models of electron-phonon interaction [23, 24], and systems in high energy physics [25–27]. One particularly interesting model is the so-called coupled cavity array (CCA) model that is made of arrays of optical or microwave cavities, in which each cavity couples to a nonlinear medium. It was shown that the CCA model can demonstrate Mott insulator (MI)-to-superfluid (SF) phase transition for cavity polaritons [28–33], in analogy to the Bose-Hubbard model [34, 35]. One advantage of analog quantum simulators over general-purposed quantum computers is that they put less stringent requirements on the quantum logic operations and are more robust against decoherence and leakage errors.

In a recent work, we proposed a multi-connected Jaynes-Cummings (JC) lattice model, which consists of arrays of alternatively coupled qubits and cavity modes [36]. This model can be constructed with superconducting systems, e.g., by connecting X-mon qubits and coplanar waveguide resonators [8]. Using the exact diagonalization method, we studied the quantum phase transition of this model in a finite-

*Corresponding author (email: ltian@ucmerced.edu)

size one-dimensional (1D) lattice. This system demonstrates phase transition from the incompressible MI phase to the gapless SF phase by varying the ratio between the left and the right qubit-cavity couplings. Moreover, the system shows the novel feature of reentrance to the MI phase from the SF phase when the coupling ratio is further increased. This reentrant behavior originates from the left-right symmetry between the couplings, and it distinguishes the multi-connected lattice model from the CCA. Note that effective cavity mode coupling and quantum magnetism were studied in interconnected qubit-cavity arrays that bear uniform or opposite couplings [37–39].

Here we study a detuned multi-connected JC lattice, exploring the role of qubit-cavity detuning in the MI-to-SF phase transition. We show that the effective onsite nonlinearity strongly depends on the detuning. By varying the detuning from large negative to large positive values, the nonlinearity can be tuned from weak to strong, compared with the magnitudes of the qubit-cavity couplings. We use the exact diagonalization method to find the many-body ground state of a 1D lattice. Then, the single-particle density matrix at commensurate fillings is calculated. Note that even though 1D bosonic systems do not possess long range order, the single-particle density matrix decays much faster in the MI phase than in the SF phase and still gives clear signature of the phase transition. We study the quantum phases for lattices with symmetric and asymmetric couplings, respectively. For symmetric couplings with the left and right couplings equal to each other, the phase transition demonstrates universal behavior that only depends on the ratio between the detuning and the coupling; whereas for asymmetric couplings, the phase transition shows more complicated behavior.

The qubit-cavity detuning can be conveniently adjusted by applying a global dc magnetic field to the SQUID loop of the X-mon qubits [8]. The magnetic field controls the energy level splitting of the qubits, and hence the detuning, over a very wide range. In comparison to varying the qubit-cavity couplings, a practical advantage of varying the detuning is to avoid additional circuit elements that could bring in serious complications in circuit design and operation.

This paper is organized as follows. In Sec. 2, we present the Hamiltonian for a multi-connected JC lattice model in a 1D array, and we analyze the effective onsite interaction and the effective hopping matrix element. The dependence of the onsite interaction on the qubit-cavity detuning is studied in detail. Sec. 3 starts with a description of our numerical method. We then present our results of the single-particle density matrix for both symmetric and asymmetric qubit-cavity couplings. Conclusions are given in Sec. 4.

2 Multi-connected JC lattice

2.1 Model

The multi-connected JC lattice model is made of alternatively connected qubits and cavities [36], as illustrated in Fig. 1(a). In a 1D configuration, each qubit couples to two neighboring cavities, one to the left and the other to the right hand side, with independent coupling constants g_l and g_r. We define a unit cell as one qubit and the cavity to its right hand side. The local Hamiltonian for the i-th unit cell has the form of a standard JC model with ($\hbar = 1$)

$$H_{JC}^i = \omega_c a_i^\dagger a_i + \frac{\omega_z}{2}\sigma_i^z + g_r\left(a_i^\dagger \sigma_i^- + \sigma_i^+ a_i\right), \quad (1)$$

where $\sigma_i^{\pm,z}$ denote the Pauli operators of the qubit, $a_i^\dagger$ (a_i) is the creation (annihilation) operator of the cavity mode, ω_c is the angular frequency of the cavity, and ω_z the energy level splitting of the qubit. The qubit-cavity detuning Δ is defined as the frequency difference between the qubit and the cavity with $\Delta = \omega_c - \omega_z$.

In addition, the qubit at site i couples to the cavity at site $i-1$ with the interaction

$$H_{int}^i = g_l\left(a_{i-1}^\dagger \sigma_i^- + \sigma_i^+ a_{i-1}\right), \quad (2)$$

which is also in the form of the JC coupling. Combining the local Hamiltonian (1) and the interaction (2), we can write the total Hamiltonian of the multi-connected JC lattice model as

$$H_t = \sum_i \left(H_{JC}^i + H_{int}^i\right), \quad (3)$$

where the summation runs over the entire lattice. It is noteworthy that the total Hamiltonian is invariant under a left-right reflection of the lattice accompanied by an exchange of the couplings g_l and g_r. This reflection symmetry is at the heart of the reentrant behavior studied in our previous work [36]. Multi-connected lattices with more complicated geometries in higher dimension can also be studied. For example, the qubits and cavities can be connected in a checkerboard pattern in a two-dimensional lattice, as illustrated in Fig. 1(b).
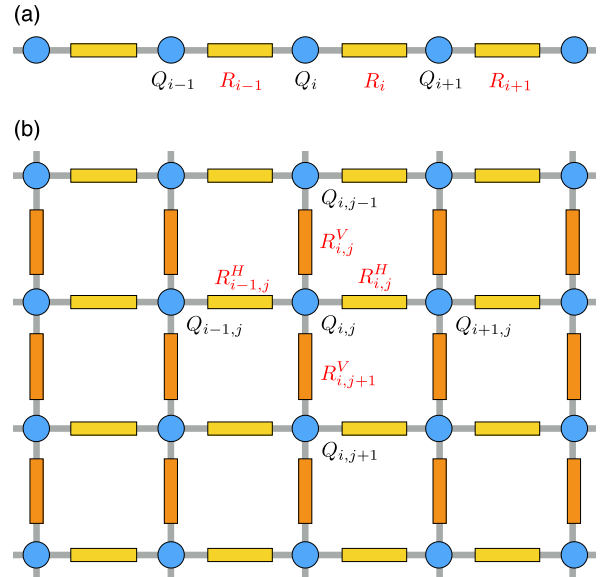

Figure 1   Multi-connected JC lattice models. (a) A 1D lattice made of alternatively connected qubits Q_i and cavities R_i. Each qubit Q_i couples simultaneously to R_i with coupling g_r and to R_{i-1} with coupling g_l. (b) A two-dimensional lattice with the qubits and the cavities connected in a checkerboard pattern. Here a unit cell consists of a qubit $Q_{i,j}$, a cavity $R_{i,j}^H$, and another cavity $R_{i,j}^V$. The qubit $Q_{i,j}$ couples to four cavities: $R_{i,j}^H$, $R_{i,j}^V$, $R_{i-1,j}^H$, and $R_{i,j+1}^V$, with respective couplings.

2.2 Nonlinearity and hopping

The total Hamiltonian H_t possesses the key elements for a MI-to-SF phase transition: an effective onsite nonlinear interaction and effective hopping matrix elements between neighboring sites. To illustrate this point, we study this model

in the strongly-asymmetric limit of $g_l \ll g_r$ (or similarly, $g_r \ll g_l$). First, we consider the local Hamiltonian H_{JC}^i at site i. The eigenstates of H_{JC}^i include a zero-excitation state $|0_i\rangle = |0, \downarrow\rangle$ and the polariton doublets $|n_i, \pm\rangle$ with

$$|n_i, +\rangle = \cos \frac{\delta_{n_i}}{2} |n_i, \downarrow\rangle + \sin \frac{\delta_{n_i}}{2} |n_i - 1, \uparrow\rangle, \quad (4a)$$

$$|n_i, -\rangle = \sin \frac{\delta_{n_i}}{2} |n_i, \downarrow\rangle - \cos \frac{\delta_{n_i}}{2} |n_i - 1, \uparrow\rangle, \quad (4b)$$

where $|\uparrow, \downarrow\rangle$ correspond to the spin up or down states of the Pauli operator σ_i^z, the n_i index on the right hand sides of the equations refers to cavity photon numbers, and the n_i index in the eigenstates $|n_i, \pm\rangle$ refers to the total number of excitations at site i that counts both spin flip and photon excitations. Here $\cos \frac{\delta_{n_i}}{2} = \sqrt{\frac{1}{2}(1 + \frac{\Delta}{\Omega_{n_i}})}$, $\sin \frac{\delta_{n_i}}{2} = \sqrt{\frac{1}{2}(1 - \frac{\Delta}{\Omega_{n_i}})}$, and $\Omega_{n_i} = \sqrt{\Delta^2 + 4g_r^2 n_i}$ is an effective Rabi frequency. The polariton doublets $|n_i, \pm_i\rangle$ are eigenstates with n_i excitations. The eigenenergies can be written as

$$\varepsilon_{n_i, \pm} = (n_i - 1/2)\omega_c \pm \Omega_{n_i}/2 \quad (5)$$

and $\varepsilon_{0_i} = -\omega_z/2$, respectively. The states $|n_i, -\rangle$ have lower energy in the n_i doublet, and are referred to as the lower polariton states. The energy difference $\Delta\varepsilon_{n_i} = \varepsilon_{n_i,-} - \varepsilon_{0_i}$ is thus the lowest energy cost to produce n_i excitations at site i.

To analyze the effective nonlinearity, we use the following estimation. Assume that the energy of lower polariton states $|n_i, -\rangle$ can be described by an effective Hamiltonian $H_{\text{eff}} = \omega_p p_i^\dagger p_i + (U/2)p_i^\dagger p_i^\dagger p_i p_i$, where ω_p is the single-polariton energy and U is the magnitude of the Hubbard on-site interaction. The energy cost to generate n_i excitations is thus $\Delta\varepsilon_{n_i} = n_i\omega_p + (U/2)n_i(n_i - 1)$, with the special case of $\Delta\varepsilon_{1_i} = \omega_p$. With these relations, the Hubbard interaction can be written as $U = (\Delta\varepsilon_{n_{i+1}} - \Delta\varepsilon_{n_i} - \omega_p)/n_i$. Combining this result with the eigenenergies given in (5), we can estimate the interaction U in terms of the detuning and the qubit-cavity coupling for selected n_i value. Note that different from the Hubbard model, the effective U in our estimation depends on n_i. The JC model cannot be exactly mapped to the Hubbard model, even though the nonlinearity is a convenient way to analyze the behavior of this system. For example, at zero detuning with $\Delta = 0$, $U = g_r(1 + \sqrt{n_i} - \sqrt{n_i + 1})/n_i$ for n_i excitations, proportional to the coupling strength g_r and decreasing monotonically with the total excitation number n_i. The dependence of U on n_i is shown in the inset of Fig. 2.

In this system, the detuning can be an effective knob to tune the phase transition between the MI and the SF phases. Practically speaking, it is easier to control the qubit-cavity detuning than to adjust the qubit-cavity couplings in the laboratory. The detuning of superconducting qubits can be controlled with global external magnetic field over a very wide range [8]. Below we study the dependence of the Hubbard U on the detuning. In Fig. 2, we plot U as functions of the detuning for low-lying polariton states with $n_i = 1$ to 10 and a coupling strength of $g_r = 150$ MHz. The nonlinearity increases continuously with the detuning. In the limit of large detuning magnitude with $|\Delta| \gg g_0$, we find that $U \approx (\Delta + |\Delta|)/2n_i$, i.e., for large positive detuning, $U \to \Delta/n_i$ and for large negative detuning, $U \to 0$. This indicates that for low-lying polariton excitations, the SF phase is more favorable at negative detuning with a nearly vanishing effective interaction; and the MI phase is more favorable at large positive detuning.
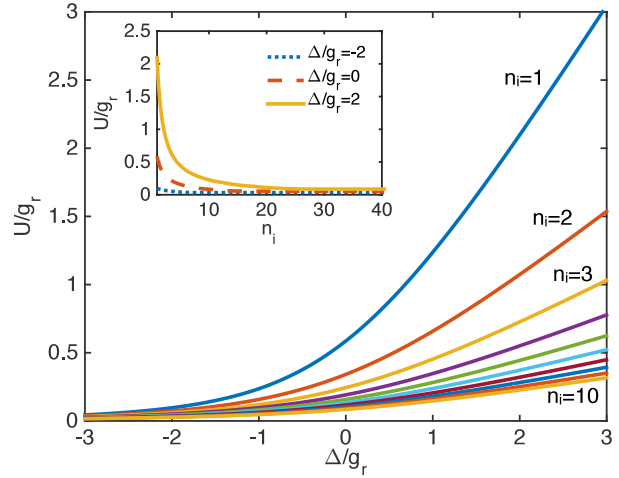

Figure 2   The effective nonlinearity U versus Δ/g_r with $g_r = 150$ MHz. Inset: U versus n_i for $\Delta/g_r = -2$, 0 and 2, respectively.

Assume the coupling g_l between neighboring sites to be finite with $g_l \ll g_r$. The coupling H_{int}^i between adjacent sites can be treated as a perturbation to the eigenstates (4a) and (4b). Consider the matrix element of H_{int}^i between state $|A\rangle = |n_{i-1}, -\rangle \otimes |n_i, -\rangle$, which contains n_{i-1} excitations at site $i - 1$ and n_i excitations at site i, and state $|B\rangle = |n_{i-1} - 1, -\rangle \otimes |n_i + 1, -\rangle$, which includes $(n_{i-1} - 1)$ excitations at site $i - 1$ and $(n_i + 1)$ excitations at site i. We find

$$\langle B|\sigma_i^+ a_{i-1}|A\rangle = -\sin \frac{\delta_{n_i}}{2} \cos \frac{\delta_{n_i+1}}{2} \times$$
$$\left(\sqrt{n_{i-1}} \sin \frac{\delta_{n_{i-1}-1}}{2} \sin \frac{\delta_{n_{i-1}}}{2} \right.$$
$$\left. + \sqrt{n_{i-1} - 1} \cos \frac{\delta_{n_{i-1}-1}}{2} \cos \frac{\delta_{n_{i-1}}}{2} \right), \quad (6)$$

which can be viewed as a hopping matrix element for polariton excitations between neighboring sites, with a hopping amplitude proportional to the coupling g_l. The total number of excitations in the lattice is preserved during the hopping process. Hence in the limit of very asymmetric couplings with $g_l \ll g_r$, the onsite coupling g_r produces an effective Hubbard U and the weak nonlocal coupling g_l produces a hopping term between adjacent lattice sites. Similar argument can be applied to the opposite limit of $g_l \gg g_r$, in which case g_r becomes the hopping perturbation and g_l yields the effective nonlinearity.

Compared with the CCA, the multi-connected JC lattice model bears the distinct feature that the cavities do not interact directly, and as a result, the hopping of the excitations is not caused by direct coupling between cavity modes. In the CCA, local qubit-cavity coupling produces onsite nonlinearity and cavity coupling induces hopping between neighboring sites. Whereas in the multi-connected JC lattice, both onsite nonlinearity and hopping are caused by the qubit-cavity couplings. In particular, when the magnitudes of the left and the right couplings are comparable ($g_l \sim g_r$), the role of each coupling cannot be simply analyzed as either inducing the nonlinearity or generating the hopping. It is the interplay between the left and the right couplings that give rise to the phase transition in this model.

3 Detuning induced phase transition

3.1 Numerical method

In this section, we study detuning-induced quantum phase transition in the multi-connected JC lattice model using the exact diagonalization method. For this purpose, we choose the basis vectors

$$|\psi\rangle = |n_1, \sigma_1\rangle \otimes |n_2, \sigma_2\rangle \cdots |n_M, \sigma_M\rangle \tag{7}$$

to construct the matrix representation of the total Hamiltonian for a finite system with lattice size M and total excitation number N. Here n_i is photon excitations, and $\sigma_i = \downarrow, \uparrow$ is the qubit state at site i with $\downarrow$ ($\uparrow$) corresponding to 0 (1) spin excitation. The operator for the total excitations in the lattice is defined as $\hat{N} = \sum_i (a_i^\dagger a_i + \sigma_i^+ \sigma_i^-)$, including both photon and spin excitations. In our model, with the commutation relation $[\hat{N}, H_t] = 0$, the total excitation number is a good quantum number. Below we study the quantum phase of many-body ground state at commensurate fillings, i.e., the total excitation number N is a multiple of the lattice size M. Hence, only these basis vectors that have N excitations are selected in the numerical calculation. Because the Hamiltonian is a sparse matrix on the selected vector space, we use a Lanczos algorithm to solve the many-body ground state $|G\rangle$. Note that we have assumed the periodic boundary condition for the lattice to ensure translational symmetry.

For a finite size system, the order parameter $\langle G|a_i|G\rangle$, which is often used to characterize quantum phase transition in the thermodynamic limit, is always equal to zero because of particle number conservation. Instead, we use the single-particle density matrix defined as

$$\rho_1(i, j) = \langle G|a_i^\dagger a_j|G\rangle / \langle G|a_i^\dagger a_i|G\rangle \tag{8}$$

to characterize the phase transition in this model. From definition, $\rho_1(i, j)$ is hermitian and semi-positive definite. Furthermore, due to the translational and reflectional symmetry of the multi-connected JC lattice under periodic boundary condition, $\rho_1(i, j)$ is also real, symmetric, and cyclic. Hence $\rho_1(i, j)$ only depends on $|i - j|$, and hereafter we write the single-particle density matrix as $\rho_1(x)$ with $x = |i - j|$. For 1D bosonic systems in the SF phase, $\rho_1(x)$ decays algebraically; whereas in the MI phase, $\rho_1(x)$ decreases exponentially to zero. Hence, $\rho_1(x)$ in the SF phase could have much larger value at finite x than that of the MI phase due to its slower decay. Note that due to the finite size effect, $\rho_1(x)$ in our calculation will not reach zero in the MI phase. It decreases to a small finite value that will be clearly distinguishable from that of the SF phase. As a result, we can verify the occurrence of the phase transition, even though we cannot accurately determine the position of the quantum critical point.

In our calculation, we choose a lattice size $M = 8$ and a total excitation number $N = 8$, with the qubit-cavity couplings in a range of 0 - 300 MHz and the qubit-cavity detuning in the range of $\Delta/g_0 \in [-3, 3]$. Here $g_0 = 150$ MHz is introduced as a unit of the detuning, with its strength comparable to the qubit-cavity couplings.

3.2 Phase transition with symmetric couplings

First, we study the detuning effect on the quantum many-body phase of a symmetric multi-connected JC lattice model, in which the left and the right qubit-cavity couplings are equal to each other with $g_l = g_r$. The many-body phase of this system thus only depends on the ratio between the detuning and

the coupling g_r. In Fig. 3, we plot the single particle density matrix $\rho_1(x = x_{max})$ as a function of the detuning Δ at the maximal lattice distance x_{max} and at selected values of the coupling g_r. Note that for the lattice size $M = 8$, $x_{max} = 4$ under the periodic boundary condition.
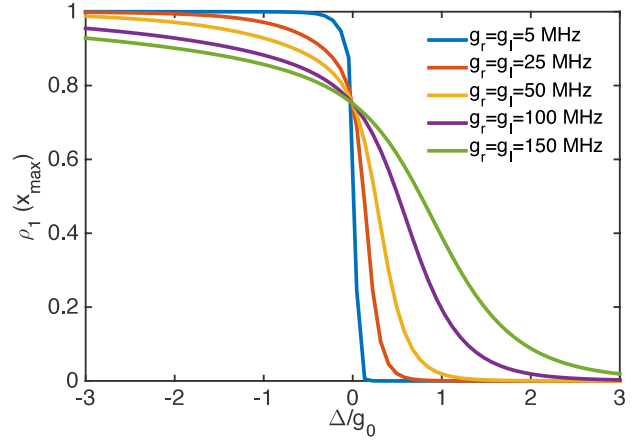

Figure 3 The single-particle density matrix $\rho_1(x = x_{max})$ versus the unitless detuning Δ/g_0 at selected couplings with $g_l = g_r$ and $g_0 = 150$ MHz.

The numerical result shows that $\rho_1(x_{max})$ decreases monotonically with the detuning. For large negative detuning with $-\Delta \gg g_r$, $\rho_1(x_{max}) \to 1$. At $\Delta = 0$, $\rho_1(x_{max}) \sim 0.75$, which is still a large finite value of the order of unity. For large positive detuning with $\Delta \gg g_r$, however, $\rho_1(x_{max}) \to 0$. The system hence exhibits a transition from the SF to the MI phases as Δ increases from negative to positive values. This result shows excellent agreement with the nonlinearity given in Fig. 2, in which the effective nonlinearity increases from nearly zero to large finite value as the detuning increases. The phase transition can be explained with an intuitive physical picture. For large negative detuning, $\omega_c \ll \omega_z$, and the lower polariton states can be approximated as photon states with equal energy spacing, i.e., having weak nonlinearity. The many-body ground state in the presence of finite qubit-cavity coupling is then a superfluid of the photons. For large positive detuning, on the other hand, $\omega_c \gg \omega_z$, and the lower polariton states are approximately the qubit states that are localized at its own site. The many-body ground state then resembles the MI phase where hopping is prohibited by large nonlinearity.

Note that for symmetric couplings, the behavior of this system depends on the ratio Δ/g_r only. Hence the curves for different g_r values in Fig. 3 can be rescaled to become one single curve. In other words, the width of the transition region between the SF and the MI phases scales with the coupling constant g_r, with wider detuning region for greater g_r value. It is also worth noting that $\rho_1(x_{max})$ at $\Delta = 0$ is independent of the coupling g_r with the system in the SF phase regardless of the coupling strength.

3.3 Phase transition with asymmetric couplings

Now we consider the detuning effect on the phase transition of asymmetric systems with distinct qubit-cavity couplings g_l and g_r. We calculate $\rho_1(x_{max})$ as a function of Δ for selected pairs of couplings as shown in Fig. 4. The couplings are chosen in the experimentally approachable regime of $g_{l,r} \in [0, 300]$ MHz and satisfy $g_l + g_r = 300$ MHz. The numerical result shows the generic feature that the single-particle density matrix $\rho_1(x_{max})$ decreases with the increase of

the detuning. In contrast to the case of symmetric couplings in Sec. 3.2, the ratio of the qubit-cavity coupling g_l/g_r plays an important role in the many-body phase of the ground state. For instance, at $(g_l, g_r) = (5, 295)$ $(g_l/g_r = 0.017)$, $\rho_1(x_{max}) \approx 0$ in the entire region of $\Delta/g_0 \in [-3, 3]$, which indicates that the system is in the MI phase. Whereas at $(g_l, g_r) = (50, 250)$ $(g_l/g_r = 0.2)$, $\rho_1(x_{max}) > 0.8$ for $\Delta/g_0 = -3$, clearly indicating that the system is in the SF phase. Hence depending on the ratio between the couplings, the phase transition can occur at either negative or positive detuning.
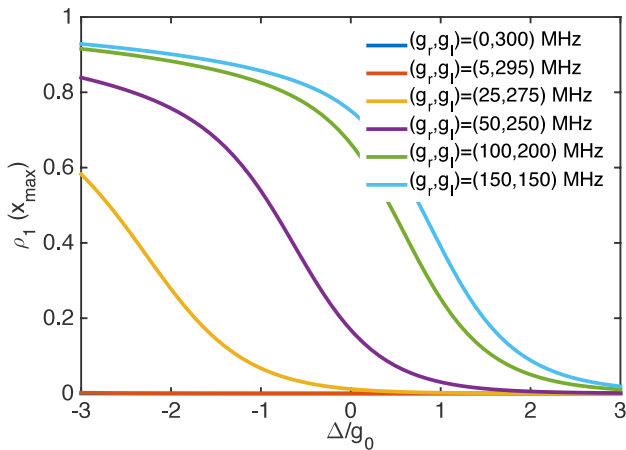

Figure 4 The single-particle density matrix $\rho_1(x = x_{max})$ versus the unitless detuning Δ/g_0 at selected pairs of couplings and $g_0 = 150$ MHz. The couplings are $(g_l, g_r) = (0, 300)$, $(5, 295)$, $(25, 275)$, $(50, 250)$, $(100, 200)$, and $(150, 150)$ MHz, respectively.

4   Conclusions

To conclude, we studied the quantum phase transition in the many-body ground state of a 1D multi-connected JC lattice model. Using a numerical method, we showed that by varying the qubit-cavity detuning, the SF-to-MI phase transition can be observed in this system. The quantum critical point not only depends on the magnitude of the couplings, but also depends on the ratio between the left and the right couplings of the lattice. Our results show that the multi-connected JC lattice model could be a rich system to explore the many-body physics of cavity polaritons.

1 Feynman R P. Simulating physics with computers. Int J Theor Phys, 1982, 21: 467
2 Georgescu I M, Ashhab S, Nori F. Quantum simulation. Rev Mod Phys, 2014, 86: 153
3 Chen Y, Roushan P, Sank D, Neill C, Lucero E, Mariantoni M, Barends R, Chiaro B, Kelly J, Megrant A, Mutus J Y, O'Malley P J J, Vainsencher A, Wenner J, White T C, Yin Y, Cleland A N, Martinis J M. Emulating weak localization using a solid-state quantum circuit. Nat Commun, 2014, 5: 5184
4 Schroer M D, Kolodrubetz M H, Kindel W F, Sandberg M, Gao J, Vissers M R, Pappas D P, Polkovnikov A, Lehnert K W. Measuring a Topological Transition in an Artificial Spin-1/2 System. Phys Rev Lett, 2014, 113: 050402
5 Roushan P, Neill C, Chen Y, Kolodrubetz M, Quintana C, Leung N, Fang M, Barends R, Campbell B, Chen Z, Chiaro B, Dunsworth A,
Jeffrey E, Kelly J, Megrant A, Mutus J, O'Malley P J J, Sank D, Vainsencher A, Wenner J, White T, Polkovnikov A, Cleland A N, Martinis J M. Observation of topological transitions in interacting quantum circuits. Nature (London), 2014, 515: 241
6 Macha P, Oelsner G, Reiner J-M, Marthaler M, André S, Schön G, Huebner U, Meyer H-G, Il'ichev E, Ustinov A V. Implementation of a quantum metamaterial using superconducting qubits. Nat Commun, 2014, 5: 5146
7 Devoret M H, Schoelkopf R J. Science, 2013, 339: 1169
8 Barends R, Kelly J, Megrant A, Sank D, Jeffrey E, Chen Y, Yin Y, Chiaro B, Mutus J, Neill C, O'Malley P, Roushan P, Wenner J, White T C, Cleland A N, Martinis J M. Coherent Josephson Qubit Suitable for Scalable Quantum Integrated Circuits. Phys Rev Lett, 2013, 111: 080502
9 Chow J M, Gambetta J M, Magesan E, Abraham D W, Cross A W, Johnson B R, Masluk N A, Ryan C A, Smolin J A, Srinivasan S J, Steffen M. Implementing a strand of a scalable fault-tolerant quantum computing fabric. Nat Commun, 2014, 5: 4015
10 Reed M D, DiCarlo L, Nigg S E, Sun L, Frunzio L, Girvin S M, Schoelkopf R J. Realization of three-qubit quantum error correction with superconducting circuits. Nature (London), 2012, 482: 382
11 Chen Y, Neill C, Roushan P, Leung N, Fang M, Barends R, Kelly J, Campbell B, Chen Z, Chiaro B, Dunsworth A, Jeffrey E, Megrant A, Mutus J Y, O'Malley P J J, Quintana C M, Sank D, Vainsencher A, Wenner J, White T C, Geller M R, Cleland A N, Martinis J M. Qubit architecture with high coherence and fast tunable coupling. Phys Rev Lett, 2014, 113: 220502
12 Srinivasan S J, Hoffman A J, Gambetta J M, Houck A A. Tunable Coupling in Circuit Quantum Electrodynamics Using a Superconducting Charge Qubit with a V-Shaped Energy Level Diagram. Phys Rev Lett, 2011, 106: 083601
13 Garc´ia-Ripoll J J, Solano E, Martin-Delgado M A. Quantum simulation of Anderson and Kondo lattices with superconducting qubits. Phys Rev B, 2008, 77: 024522
14 Tian L. Circuit QED and Sudden Phase Switching in a Superconducting Qubit Array. Phys Rev Lett, 2010, 105: 167001
15 Viehmann O, von Delft J, Marquardt F. Observing the Nonequilibrium Dynamics of the Quantum Transverse-Field Ising Chain in Circuit QED. Phys Rev Lett, 2013, 110: 030601
16 You H, Geller M R, Stancil P C. Simulating the transverse Ising model on a quantum computer: Error correction with the surface code. Phys Rev A, 2013, 87: 032341
17 Zhang Y, Yu L, Liang J-Q, Chen G, Jia S, Nori F. Quantum phases in circuit QED with a superconducting qubit array. Sci Rep, 2014, 4: 4083
18 Las Heras U, Mezzacapo A, Lamata L, Filipp S, Wallraff A, Solano E. Digital Quantum Simulation of Spin Systems in Superconducting Circuits. Phys Rev Lett, 2014, 112: 200501
19 Tsomokos D I, Ashhab S, Nori F. Using superconducting qubit circuits to engineer exotic lattice systems. Phys Rev A, 2010, 82: 052311
20 You J Q, Wang Z D, Zhang W, Nori F. Encoding a qubit with Majorana modes in superconducting circuits. Sci Rep, 2014, 4: 5535
21 Hayward A L C, Martin A M, Greentree A D. Fractional Quantum Hall Physics in Jaynes-Cummings-Hubbard Lattices. Phys Rev Lett, 2012, 108: 223602
22 Schmidt T L, Nunnenkamp A, Bruder C. Majorana Qubit Rotations in Microwave Cavities. Phys Rev Lett, 2013, 110: 107006
23 Mei F, Stojanović V M, Siddiqi I, Tian L. Analog superconducting quantum simulator for Holstein polarons. Phys Rev B, 2013, 88: 224502
24 Stojanović V M, Vanević M, Demler E, Tian L. Transmon-based simulator of nonlocal electron-phonon coupling: A platform for observing sharp small-polaron transitions. Phys Rev B, 2014, 89: 144508
25 Kapit E. Quantum simulation architecture for lattice bosons in arbitrary, tunable, external gauge fields. Phys Rev A, 2013, 87: 062336
26 Marcos D, Rabl P, Rico E, Zoller P. Superconducting Circuits for Quantum Simulation of Dynamical Gauge Fields. Phys Rev Lett, 2013, 111: 110504
27 Peropadre B, Zueco D, Wulschner F, Deppe F, Marx A, Gross R, Garc´ia-Ripoll J J. Tunable coupling engineering between superconducting resonators: From sidebands to effective gauge fields. Phys Rev B, 2013, 87: 134504
28 Hartmann M J, Brandão F G S L, Plenio M B. Strongly interacting polaritons in coupled arrays of cavities. Nature Phys, 2006, 2: 849
29 Greentree A D, Tahan C, Cole J H, Hollenberg L C L. Quantum phase

transitions of light. Nature Phys, 2006, 2: 856

30 Angelakis D G, Santos M F, Bose S. Photon-blockade-induced Mott transitions and *XY* spin models in coupled cavity arrays. Phys Rev A, 2007, 76: 031805(R)

31 Na N, Utsunomiya S, Tian L, Yamamoto Y. Strongly correlated polaritons in a two-dimensional array of photonic crystal microcavities. Phys Rev A, 2008, 77: 031803(R)

32 Hartmann M J, Brandão F G S L, Plenio M B. Quantum many-body phenomena in coupled cavity arrays. Laser & Photon Rev, 2008, 2: 527

33 Koch J, Le Hur K. SuperfluidMott-insulator transition of light in the Jaynes-Cummings lattice. Phys Rev A, 2009, 80: 023811

34 Fisher M P A, Weichman P B, Grinstein G, Fisher D S. Boson local-

ization and the superfluid-insulator transition. Phys Rev B, 1989, 40: 546

35 Batrouni G G, Scalettar R T, Zimanyi G T. Quantum critical phenomena in one-dimensional Bose systems. Phys Rev Lett, 1990, 65: 1765

36 Seo K, Tian L. Quantum Phase Transition in A Multi-connected Superconducting Jaynes-Cummings Lattice. arXiv:1408.2304

37 Qiu Y, Xiong W, Tian L, You J Q. Coupling spin ensembles via superconducting flux qubits. Phys Rev A, 2014, 89: 042321

38 Kurcz A, Bermudez A, Garc´ia-Ripoll J J. Hybrid Quantum Magnetism in Circuit QED: From Spin-Photon Waves to Many-Body Spectroscopy. Phys Rev Lett, 2014, 112: 180405

39 Kurcz A, Garcia-Ripoll J J, Bermudez A. The Interspersed Spin Boson Lattice Model. arXiv:1408.1878